Influence of free water on concrete triaxial behavior: The effect of porosity

Yann Malecot, Ludovic Zingg, Matthieu Briffaut, Julien Baroth

Influence of free water on concrete triaxial behavior: the effect of porosity

Yann MALECOT[a], Ludovic ZINGG[a], Matthieu BRIFFAUT[a], Julien BAROTH[a]

[a] Univ. Grenoble Alpes, CNRS, Grenoble INP[1], 3SR, 38000 Grenoble, France

Corresponding author: yann.malecot@univ-grenoble-alpes.fr

ABSTRACT: *This work examines the effect of porosity and free water on the behavior of concrete under high confinement. For this purpose, three types of concretes are designed with either low, medium or high porosities but featuring the same aggregate skeleton, yielding: an ordinary referenced concrete (OC), as already characterized in previous studies; a high performance concrete (HPC) with very low capillary porosity; and a low performance concrete (LPC) with the same composition as OC except for a much higher entrained air porosity. The results of triaxial tests, conducted on these three concretes up to a confinement of 600 MPa at both low and high saturation ratios, are presented. The conclusions from past studies on OC are extended herein for the cases of HPC and LPC: the free water quantity exerts a major influence on the concrete strength capacity as well as the volumetric stiffness for all three types of concretes. These results also show that the free water influence on concrete behavior depends on both the amount and nature of this porosity: the effect of modifying the entrained air porosity is much weaker than that of capillary porosity. To better quantify the effect of concrete saturation ratio, results are then completed by triaxial testing performed on OC with intermediate saturation ratios. Lastly, an empirical triaxial failure criterion of concrete, which takes into account the uniaxial strength, porosity and saturation ratio, is proposed; this new criterion accurately reproduces the results presented, as well as, a large database obtained from previous studies.*

Keywords: *high confinement, triaxial test, saturation ratio, concrete, porosity, free water.*

1. Introduction

This paper examines the influence of free water on concrete triaxial behavior under very high confinement. In the presence of impact or ~~blast loading~~ near-field explosion, massive concrete structures may be subjected to high triaxial compressive stresses [1]. For instance, mean stress levels of approx. 1 GPa were measured in a concrete slab struck by a steel projectile (50-mm diameter, 2.3 kg) launched at 315 m/s [2]. Thus, to develop numerical models able to simulate impacts on concrete structures, the characterization and modeling of triaxial behavior of concrete under high stress level, is still of growing interest in literature in recent years [39-44]. Moreover, throughout their lifetime, concrete structures undergo large variations, in both space and time, of the free water quantity present in concrete porosity. From quasi-saturated after setting, concrete in most cases is exposed to an environment with lower relative humidity, resulting in a drying process occurring within the material. The time required to reach moisture equilibrium varies with the square of structural thickness [3]. For massive structures such as dams, nuclear reactors or protective structures, their core could remain quasi-saturated throughout most of their lifetime, even though their facing dries very quickly. The dependence of concrete behavior on saturation ratio thus constitutes an important research topic widely investigated in the literature. Wang *et al.* [4] carried out static and dynamic triaxial tests on dam concrete and showed that saturated

[1] *Institute of Engineering Univ. Grenoble Alpes*

concrete is more strain rate sensitive than dry concrete. The authors attributed this dissimilarity to the viscosity of pore water circulating inside the saturated concrete during quasi-static or dynamic loading. Zhou *et al.* [5] also studied the influence of free water content on the compressive mechanical behavior of cement mortar under a high strain rate. They found that the dynamic compressive strength of saturated specimens was 23% less than that of fully dried specimens. Forquin *et al.* [6] and Piotrowska *et al.* [7] assessed the influence of free water on the oedometric behavior of concrete with both quasi-static and dynamic loading rates.

To better evaluate the vulnerability of massive concrete structures under extreme loading conditions, a partnership between the Université Grenoble Alpes (3SR Laboratory) and the CEA Gramat was launched in 2004. This partnership led to the design of a triaxial press with high loading capacities, called GIGA, to determine the behavior of concrete under high confinement. In using this press, several studies were conducted over the past decade on specimens made of the same baseline material in order to refine understanding of the triaxial behavior of concrete [8-14]. More specifically, these past studies served to quantify the influence of the water/cement (*W/C*) ratio [8] and the saturation ratio S_r [15] on the confined behavior of an ordinary concrete. Two major results could be derived:

a) Under very high confinement, concrete behaves like a non-cohesive granular stacking, on which the cement matrix strength of the sound concrete seems to exert no influence; this stacking becomes insensitive to the uniaxial compressive strength of concrete f_{ck}, which appears to be a poor indicator of the high-pressure mechanical response of concrete [8] when the saturation ratio of the material is dry enough. Previously obtained for ordinary concretes without admixtures, this result has recently been extended to both high performance concrete (HPC) with very low capillary porosity and low performance concrete (LPC) with high entrained air porosity [14]. This result proves to be critical since *W/C* is the main parameter of the concrete composition controlling f_{ck}. Moreover, f_{ck} is often the only physical parameter characterizing the concrete triaxial strength in building codes [16, 17] or in triaxial behavior models [8, 18].

b) The saturation ratio exerts a major influence, particularly on both the concrete strength capacity and volumetric stiffness: while an increase in volumetric stiffness is observed with an increase in saturation ratio, a very strong decrease in deviatoric strength capacity is observed in the same time. The maximum shear stress of concrete can be divided by 5 for a saturated state compared to a dry state (Sr = 10%) [11].

The purpose of this paper is to assess the influence of free water on the triaxial behavior of concrete on specimens with different porosity ratios and types. The specific objectives of this paper are described in the three following points:

(i) Is the (b) result, as regards the strong influence of water, obtained on ordinary concrete, is extendable to high performance concretes (HPC) with very low capillary porosity or to concretes with a high entrained air porosity (i.e. concrete that can withstand freeze-thaw cycles)? The issue behind this question is important in terms of a fundamental understanding of physical phenomena as well as from an industrial perspective. A better understanding of the influence of water for each type of porosity will indeed lead to an improved characterization of the concretes used in construction projects over the past 30 years.

(ii) Since the saturation ratio of concrete structures varies from a quasi-dry state on the outer surfaces to a quasi-saturated state at the core, the most typical state for concrete is "wet". It is thus necessary to characterize the behavior of concrete under high stress levels for intermediate saturation ratios. In this study, the behavior of concrete for intermediate saturation ratios has been evaluated using climatic chambers to ensure a precise control over the concrete free water content, which was not the case for previous results found in the literature.

(iii) In most concrete triaxial behavior models or building codes, the unconfined compressive strength is the only physical parameter characterizing concrete strength. To facilitate the improvement of such models, an analytical triaxial failure criterion of concrete, based on experimental results from this study and past works, which accounts for both saturation ratio and porosity, will be proposed.

After an initial section presenting the experimental set-up and concrete mix designs implemented in this study, the three previous points will be treated sequentially in the subsequent sections of the paper.

Notations

Variables

f_{ck}	Uniaxial unconfined compressive strength
E	Young's modulus
S_r	Saturation ratio
p	Confining pressure
ε	Strain
ε_V	Volumetric strain
ε_{V^*}	Critical volumetric strain
σ_x	Principal axial stress
σ_0	Reference mean stress
σ_m	Mean stress
$\sigma_{c_{sat}}$	Critical mean stress level
$\sigma_{c_{p0}}$	Ultimate consolidation stress
λ, κ	Parameters controlling the decrease of $\sigma_{c_{sat}}$

Sign conventions

$\varepsilon > 0$	during contraction
$\sigma > 0$	during compression

m_{sat}	Weight of the saturated sample
m_{sr}	Weight of the sample after stabilization
m_{hyd}	Weight of the saturated sample in water
Φ_w	Porosity of the concrete accessible to water
Φ_{cap}	Capillarity porosity
Φ_{air}	Entrained air porosity
q	Deviatoric stress ($q = \sigma x - p$)
q_1	Critical shear stress
q_{max}	Maximum deviatoric stress capacity of a sample
$q_{max,dry}$	q_{max} for dry samples
$q_{max,sat}$	q_{max} for saturated samples
q_{sat}	Upper limit of q_{max} for a saturated concrete
q_{sr}	Upper limit of q_{max} for a wet concrete (Sr)
q_0	Upper limit of q_{max} for a dry concrete (S_r=0%)

Abbreviations

REV	Representative Elementary Volume
HPC	High Performance Concrete
LPC	Low Performance Concrete
OC	Ordinary Concrete

2. Experimental program

2.1. Composition of the concrete mixes

All concrete mixes and main properties have been listed in Table 1. The ordinary concrete (OC), called R30A7 in previous studies, displays a 28-day unconfined compressive strength f_{ck} of approx. 30 MPa and a slump of 7 cm. Two specimens, one of low performance concrete (LPC) the other of high performance concrete (HPC), have been composed in an attempt to resemble the OC mix design as closely as possible in terms of their granular skeleton [10]. For LPC, the entrained air porosity has been increased through use of an entrained air agent. For the HPC material, the composition mix quantities have been slightly modified. This concrete has been mixed according to the Sherbrooke University method [19]. To introduce high strength and reduce capillarity porosity, the W/C ratio has been set at 0.3 thanks to use of a superplasticizer. This W/C ratio corresponds to a uniaxial compressive strength f_{ck} at 28 days of approx. 80 MPa. The capillary porosity has also been decreased by adding silica fume. A silica fume mass of about 10% of the cement mass has been chosen, as recommended by De Larrard [20], in order to avoid having to change the water mass. The quantity of sand has been reduced accordingly to conserve the same total granular skeleton mass (see Table 1).

Table 1: Concrete mix and main properties of the studied concretes [10]

Concrete mix (for 1 m^3)	**LPC**	**OC (R30A7)**	**HPC**
Gravel (0.5/8 mm) (kg)	1008	1008	1008
Sand (1.8 mm) (kg)	838	838	795.4
Water (kg)	169	169	140
Cement CEM II B 42.5 (kg)	263	263	420
Silica fume (kg/m^3)	-	-	46.7
Entrained air agent (kg/m^3)	0.13	-	-
Superplasticizer (kg)	-	-	4.7
Density (kg/m^3)	2278	2277	2415
Slump	120	70	> 200
Uniaxial compressive strength at 28 days f_{ck} (MPa)	24	28.6	80
Accessible porosity to water (%)	10.8	11.8	8.8
Porosity measured by mercury intrusion (at 400 MPa)	15.6	12.6	8.7
Entrapped air (measured on fresh concrete)	8.5	3.4	4.5
Water/cement ratio	0.6	0.64	0.3

The concrete mix changes introduced into LPC and HPC, compared to the OC reference, are not supposed to affect the same type of porosity. According to the definition of concrete porosity scales proposed by Metah [21], the HPC porosity should be lowest on the capillary void scale (between 0.01 and 1 µm) due to both the *W/C* ratio reduction and the use of silica fume, whereas the LPC porosity should be highest on the higher porosity scale (between 100 µm and 1 mm). Even though the concrete porosity size distribution measured by means of mercury intrusion has created controversy in the literature [22], the results of such measurements performed on these three types of concrete have

been presented in Figure 1. This figure clearly shows that the modified porosity scales are dissimilar. For HPC, the porosity decrease appears on this figure at a scale matching the definition by Metah [21], whereas for LPC the porosity increase appears at a scale of roughly 1 µm, which is much lower than expected. This difference is probably due to use of the measurement method by mercury intrusion, which requires percolating through finer porosity to fill the non-interconnected entrained air bubbles.

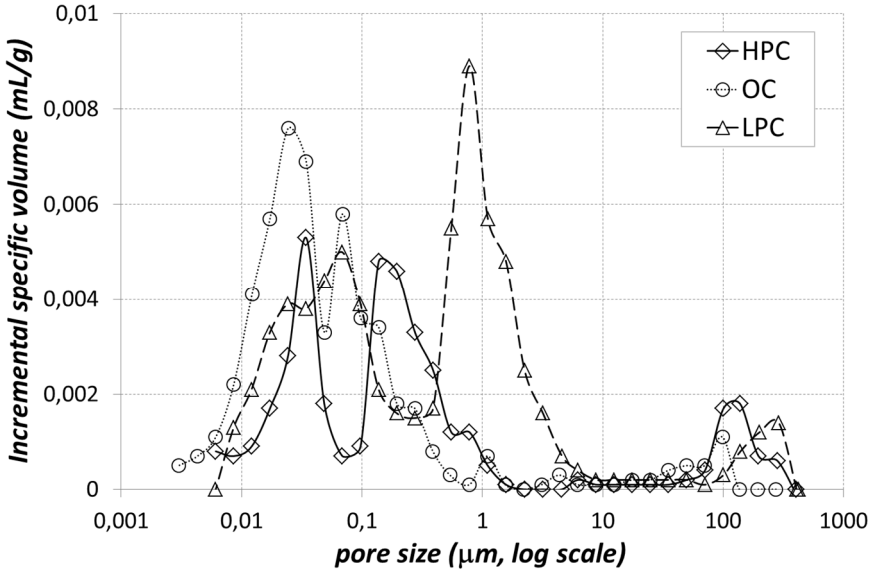

Fig. 1: Concrete porosity size distributions measured by means of mercury intrusion for OC, LPC and HPC [10]

2.2. Specimen production and conservation

Concrete specimens were cast in a parallelepiped mold with batch volumes of 13.5 liters (27 x 27 x 18.5 cm^3). Concrete placement entails 30 s of vibration on a vibrating table. The concrete block, upon removal from the mold 24 h after casting, was stored for 28 days in a saturated environment. All samples (70 mm in diameter and 140 mm high) were then cored and rectified with water, in order to prevent edge effects due to their geometrical defects [13].

To study the behavior of concrete at intermediate saturation ratios (i.e. between 10% and 100%), as compared to previous studies, special attention has been paid herein to ensuring good homogeneity of sample wetness. The concrete samples, saturated and already machined, were conserved at a constant temperature (T = 20°C) in sealed enclosures containing chemical salts to allow establishing a given relative humidity, as shown in Fig. 2a. A scale was placed inside the sealed enclosures to track the sample mass until stabilization. The saturation ratio S_r of a sample with a stabilized mass m_{sr} is given by:

$$S_r = 1 - \frac{m_{sat} - m_{sr}}{\phi_w (m_{sat} - m_{hyd})} \quad (1)$$

where m_{sat} is the mass of the saturated sample, m_{hyd} the mass of the saturated sample measured in water (hydrostatic weighting), and Φ_w the concrete porosity accessible to water.

Three salts corresponding to three relative humidity rates (*RH*=98%, 85% and 59%) were chosen. Fig. 2b presents the isotherm desorption curve (i.e. the evolution in saturation ratio versus relative humidity) obtained in the work by Burlion *et al.* [23-24]. Equilibrium states (S_r = 93%, 78% and 44%) corresponding to the three previous RH values, plotted with circles in Fig. 2b, lie close to Burlion's results.

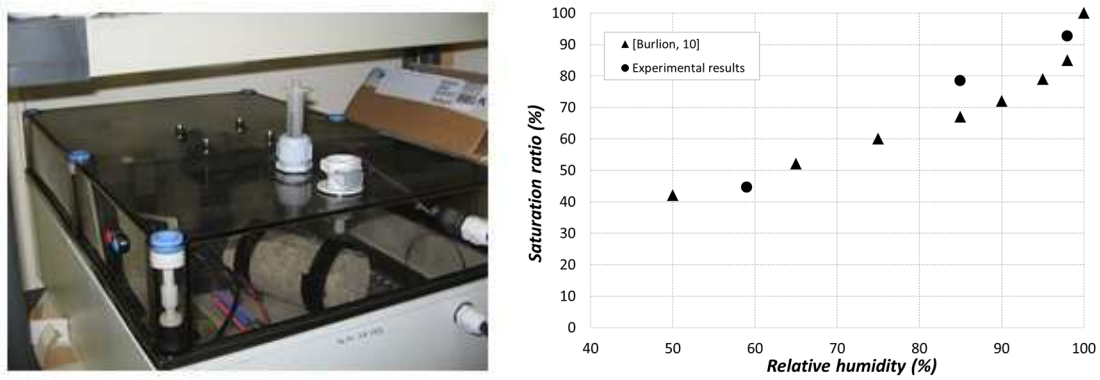

(a) (b)

Fig. 2: Experimental device to control saturation ratios (a); and desorption isotherm curve [24] (b)

2.3. Description of the GIGA press and experimental set-up

The GIGA press was designed to study the behavior of concrete under high confinement within the framework of a partnership between the Université Grenoble Alpes (3SR Laboratory) and the CEA Gramat. This press allows reaching a confining pressure of up to 0.85 GPa and an axial force of 9 MN. The experimental device is detailed in [13].

In the following discussion, σ_x is the principal axial stress, p the pressure inside the confining cell, $\sigma_m = (\sigma_x + 2p)/3$ the mean stress and $q = \sigma_x - p$ the deviatoric stress (principal stress difference). Compressive stresses and contraction strains are all assumed to be positive. All tests were conducted by following the same type of loading path. The triaxial compression test began with a hydrostatic test (uniform confining pressure around the specimen) with a constant pressure rate increase equal to 1.7 MPa/s. Then, once the desired confinement had been reached, the specimen was loaded axially (at 20 µm/s, i.e. for a strain rate of around 10^{-4}/s) while holding the confining pressure constant (see [11] for further details). To preserve the sample saturation ratio, it was necessary to limit the exposure to air-drying during sample preparation, thus preventing gluing gauges onto the samples. An LVDT sensor and a special radial sensor (developed in [25]) were used to measure axial and radial strains, respectively.

3. Hydrostatic behavior of concrete samples

Fig. 3 presents the experimental results of hydrostatic tests, up to 600 MPa, on concrete samples with a saturation ratio of approx. 10% (dry samples) for the high performance concrete (HPC), ordinary concrete (OC) and low performance concrete (LPC). As expected, the increase of mean stress σ_m vs. volumetric strain ε_V shows that the volumetric

compaction is much greater for the concrete with the highest porosity (LPC, $\varepsilon_V = 14\%$ for $\sigma_m = 600$ MPa), compared to the sample with the lowest porosity (HPC, $\varepsilon_V = 7\%$ for $\sigma_m = 600$ MPa). This kind of behavior has already been observed for other materials at lower confining pressures [26], besides, the effect of a change of the capillary porosity alone was studied by VU [8] who compared 3 concrete compositions using three different Water/Cement ratios. Results published in [8] have shown that the change of capillary porosity mainly affect the beginning of the hydrostatic behaviour of concrete (below mean stress level of 400MPa) while, according to Figure 3, the change of entrained air porosity that exists between OC and LPC changes the response of the material at least up to mean stress level of 600MPa. One could conclude from this difference in behavior that a large part of the capillary porosity is closed at the beginning of the compaction phase of concrete while the compaction of the entrained air porosity is "less easier" and spread on a larger range of mean stress levels. This result is coherent with observations that where done by Poinard [38].

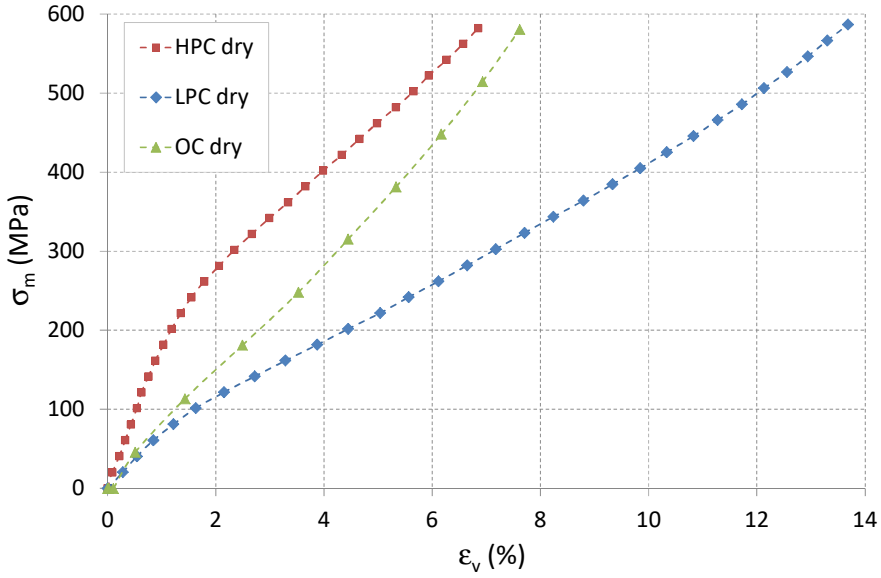

Fig. 3: Hydrostatic behavior for OC, LPC and HPC (dry specimens: Sr of approx. 10%)

Fig. 4 presents the evolution in mean stresses σ_m vs. volumetric strains ε_V for HPC, OC and LPC concretes, at both high and low saturation ratios. Regardless of the concrete type, the same trends can be identified, namely:

- 1st phase (elastic): during the elastic phase of the behavior, the effect of free water seems to be very weak while the curves are nearly identical.
- 2nd phase (damage): after the elastic phase, a decrease in the tangent bulk modulus can be observed for all three concretes. This decrease, which reflects the material damage under hydrostatic loading, is more pronounced for concretes with higher porosity. During this phase, the saturated concrete samples have a slightly softer behavior compared to the dry samples. This difference in behavior might be due to viscous effects at the scale of cement hydrates~~, with the presence of water making these hydrates softer~~. Indeed, the capillary porosity (the smallest)

being closed first compared to the entrained air porosity (the largest), one can assume that the pore closure creates an heterogeneous pore pressure field that generates water flow at microscale in the saturated samples. These water displacements that are present even under hydrostatic loading and that does not exist in dry concrete samples could generate some additional strain.

- 3rd phase (consolidation): as the mean stress level increases, the porosity decline and material densification lead to an inflection point that defines the beginning of the consolidation phase (increase in the tangent bulk modulus). This transition occurs earlier (in terms of volumetric strains) for concretes with higher porosity. Depending on the concrete type, this transition is reached between 150 and 300 MPa for dry specimens, while for saturated specimens it systematically appears at a lower mean stress level. Let's also note that beyond the inflection point, the curvature becomes more pronounced when the concrete is saturated. This strong increase of the bulk modulus observed in the 3rd phase for the saturated samples is probably due to a combination of the pore closure, that leads to an increase of the interstitial pressure, and a simultaneous increase of the bulk modulus of the water which is almost doubled between atmospheric pressure (K_w=2.25GPa) and 300MPa (K_w=4.4GPa). A simple model was proposed by Vu to reproduce this phenomenon [15]. As the level of confinement increases, the volumetric strain of saturated concretes thus becomes much lower than that of dry concretes. The strain at which the curves intersect is denoted ε_{V^*} and called the critical volumetric strain. As ε_{V^*} increases with concrete porosity, which yields three distinct values of ε_{V^*} for the three concretes (see Fig. 4), each of these values coincides with a mean stress level right around 300 MPa.

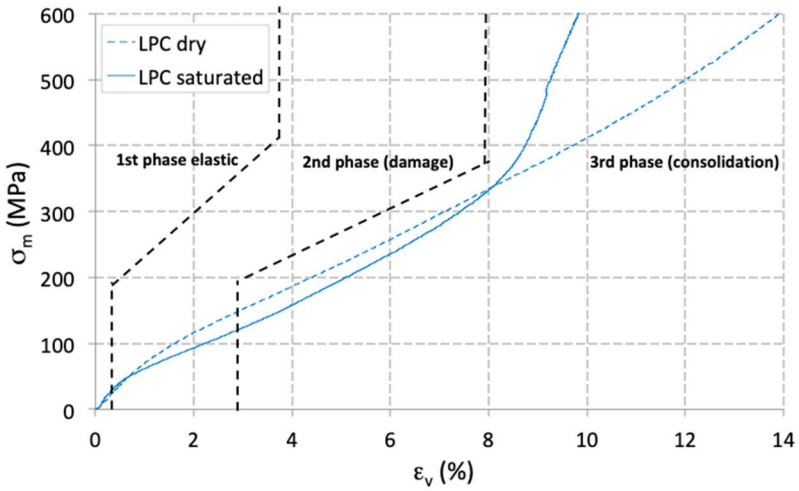

(a)

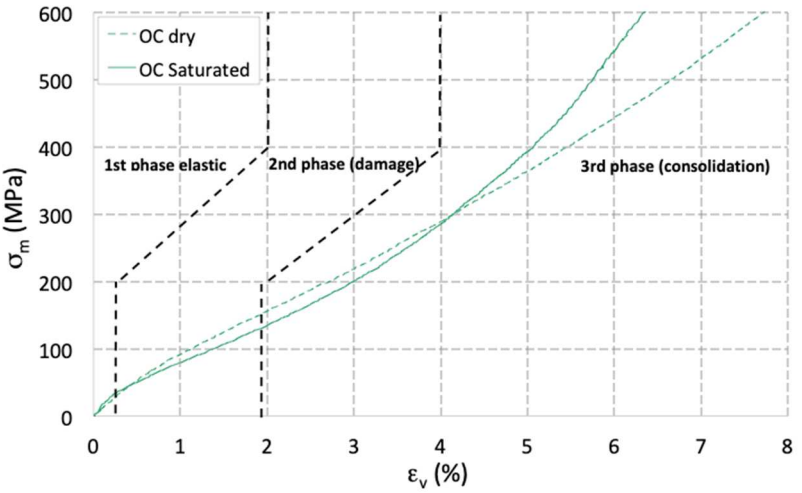

(b)

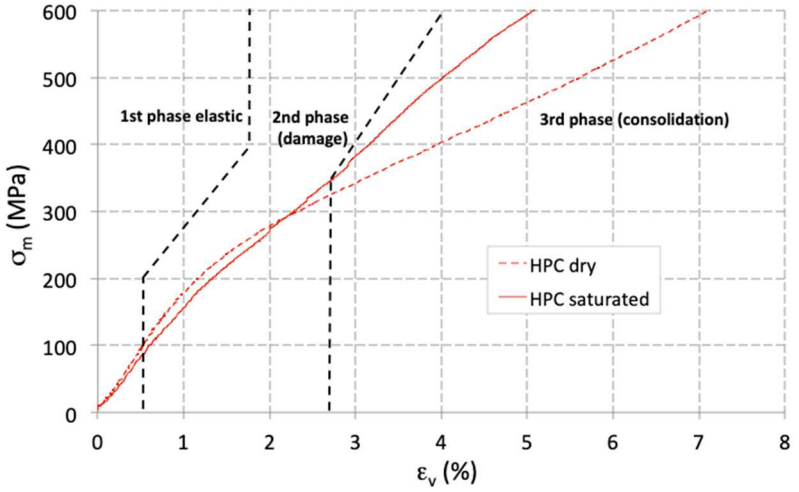

(c)

Fig. 4: Effect of saturation on hydrostatic behavior for high porosity concrete LPC $\varepsilon_{V^*} = 8\%$ (a); ordinary concrete OC $\varepsilon_{V^*} = 4\%$ (b); and low porosity concrete HPC $\varepsilon_{V^*} = 2.2\%$ (c)

The hardening of the volumetric behavior, which occurs beyond ε_{V^*}, probably results from pressurization of the free water associated with pores closing. This phenomenon has already been observed and modeled for OC concrete [15]. With a simplified poromechanical approach, it can be assumed that the mean stress difference between the dry and saturated behavior is equal to the product of the Biot coefficient and the interstitial water pressure [27]. Since both the Biot coefficient and interstitial pressure values are greater for larger concrete pores, the hardening phase more readily apparent for concretes with the highest porosity (Fig. 4). However, it is probable that the Biot coefficient value, which differs substantially among the three concretes at the beginning of loading, tends to converge under high stress levels due to the closure of pores, thus limiting the differences in hardening observed across the three concretes.

4. Deviatoric behavior of concrete samples

Fig. 5 shows the trends in deviatoric stresses q vs. axial strain ε_x for confining pressures of 50, 200 and 600 MPa during triaxial tests conducted on HPC and LPC. While HPC shows higher deviatoric stresses compared to LPC, at low confinement stresses, the behaviors of LPC and HPC at high confinement are very similar. Indeed, under very high confinement, the cement matrix of the concrete loses its cohesion, and the behaviour is influenced to a lesser extent by the cement matrix strength. Moreover, the decrease in porosity leads to higher density and the behaviour then is being essentially governed by the granular compacted stacking of the concretes. Since the granular skeletons of HPC and LPC are close, a similar deviatoric behaviour is observed (see [10] for more details).

Regardless of concrete type, at low confining pressure, the saturation effect remains slight, and the behavior of dry or saturated concrete is very similar. Looking closely at the curves of HPC, higher deviatoric stresses in saturated concrete at similar strains (up to about 4%) are however observed for high confining stresses. This is due to a stiffer behavior of saturated HPC at the beginning of the deviatoric phase (which just follows the end of hydrostatic phase). This observation is coherent with the results shown on Fig. 4, which show that beyond a mean stress of 200MPa saturated HPC samples are stiffer than the dry ones in term of bulk modulus.

In contrast, under high confining pressure beyond a ~~critical~~ given deviatoric stress, q_{max}, a plateau is reached for saturated samples whereas dry specimens exhibit a strong positive hardening until the end of the test where q_{max} is reached. For saturated samples, this ~~critical stress~~ maximum deviatoric stress capacity, q_{max}, is inversely related to porosity, i.e. lower for LPC (Fig. 5a) than for HPC (Fig. 5b). Hence, for intermediate confining pressures like 200 MPa, the effect of the saturation ratio on behavior is insignificant for HPC while already highly significant for LPC.

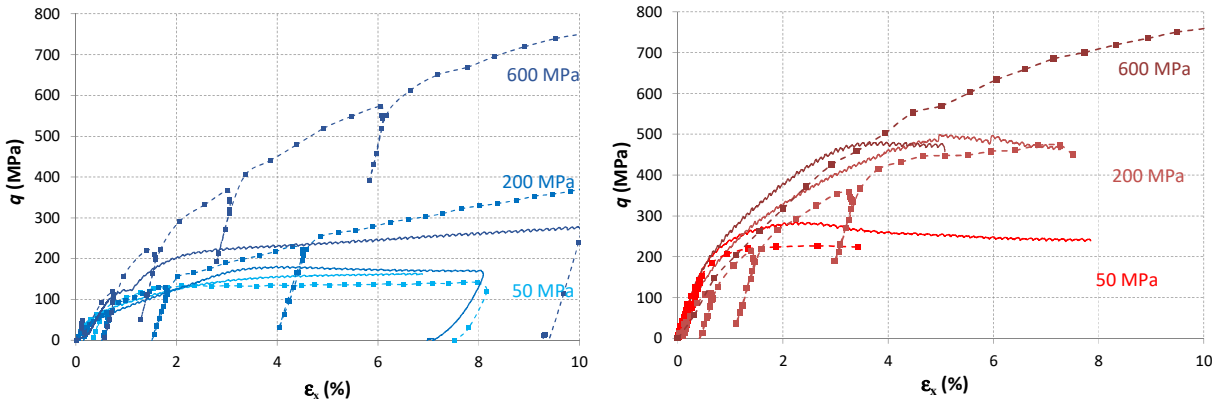

Fig. 5: Deviatoric stress vs. axial strain at various confining pressures: low performance concrete (a) and high performance concrete (b) for both dry specimens (dashed lines with square) and saturated specimens (solid lines)

Fig. 6 displays the evolution in deviatoric stress q vs. axial strain ε_x for HPC, OC and LPC concretes, in both dry and saturated states yet at the same confining pressure (equal to 400 MPa). A greater effect of free water is observed on concrete with higher capillary porosity (LPC and OC) relative to HPC. The maximum deviatoric stress reached equals 200 MPa for LPC and OC as opposed to 500 MPa for HPC. The lower cement paste cohesion acts to increase the effect of free water. These results are consistent with Biot coefficient increases as the cement matrix porosity increases. For dry concrete, even though the deviatoric behavior follows this same trend, the limit deviatoric stress seems to tend to a slightly lower value for HPC. A gap between the saturation ratios of the different concretes could provide an explanation. The same curing conditions (temperature and relative humidity) are actually applied to all three concretes, leading to higher residual saturation for a lower concrete permeability.

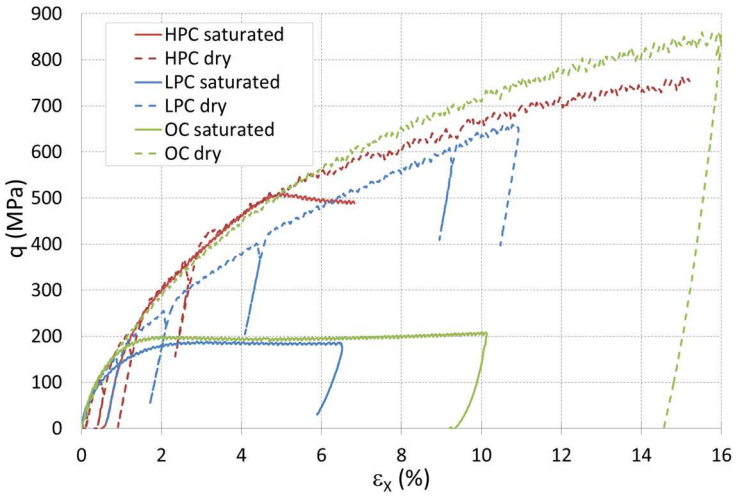

Fig. 6: Comparison of deviatoric behavior for the three concretes under study (LPC, OC, HPC) under a confining pressure of 400 MPa, for two saturation states (dashed lines for dry, and solid lines for saturated)

5. Limit states ~~and failure pattern~~

During the experimental characterization of geomaterials, various criteria may be used to identify their limit state curve. In this paper we will consider, as limit state, the stress state associated with the maximum deviatoric stress q_{max} that the concrete can support (i.e. the stress limit state). Note that in all the presented tests, this stress limit state lies close to the stress state associated with the transition point from material contraction to dilatancy. Fig. 7 plots the evolution in maximum deviatoric stress q_{max} vs. mean stress σ_m for OC. These limit states are complementary to those estimated in [11] on the same concrete. In this latter study, the limit states were observed for specimens with a heterogeneous saturation ratio. Fig. 7 also presents new deviatoric stress limit values for homogeneous samples with Sr = 78% (i.e. around 330-350 MPa) and Sr = 44% (deviatoric stress around 600 MPa).

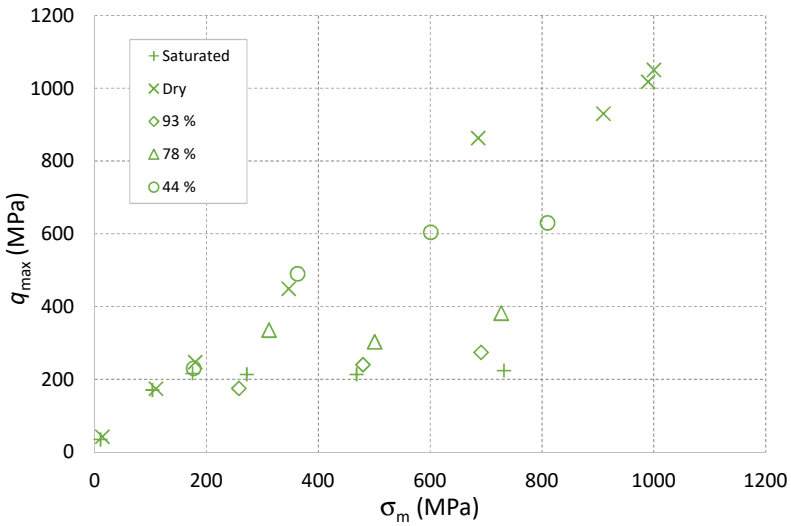

Fig. 7: Limit state curves of maximum deviatoric stress q_{max} vs. mean stress σ_m, for OC, at 5 saturation states

The upper limit of q_{max}, q_{sr} (varying from q_0 to q_{sat}) ~~limit deviatoric stress~~ can now be plotted with respect to the saturation ratio for OC (Fig. 8). It should be noted that the dry state cannot physically correspond to a saturation ratio equal to 0 but instead has been estimated in this study at about 10%. A nonlinear trend is observed, especially for low saturation ratios, as will be discussed in detail in Section 6. The regression curve used in Fig. 8 is shown for the sake of illustration herein and will also be discussed in Section 6. The ~~theoretical~~ Y-axis intercept, q_0, should match the stress state (σ_m , q_{max}) in which porosity tends to zero for a dry concrete (total consolidation point) and seems to tend to approx. 1216 MPa for OC. Let's recall however that the press capacity does not provide a clear observation of the highest plateau, even for a dry sample (i.e. an Sr around 10%).

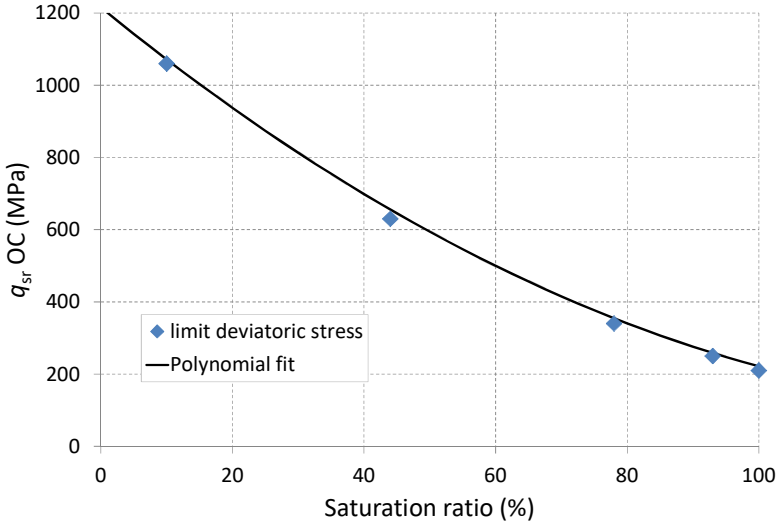

Fig. 8: Upper limit of the maximum deviatoric stress vs. saturation ratio for OC

Fig. 9 graphs the evolution in maximum deviatoric stress q_{max} vs. mean stress σ_m for: LPC (with highest porosity) (a), HPC (with lowest porosity) (b), under both dry and saturated states. One result, as already presented in [9], suggests that dry concretes tend to behave similarly under very high confinement, namely like a non-cohesive granular stacking: the cement matrix loses all its cohesion. The new result in Fig. 9 clearly shows the limit states for saturated concretes at around 200 and 500 MPa for the maximum deviatoric stress values of LPC and HPC, respectively. It is also worth noting that LPC and OC reveal nearly the same limit state, even if the porosity measured by means of mercury intrusion at 400 MPa was respectively 15.6% and 11.8% for LPC and OC (for a difference of some 25%, see Table 1). The loss of porosity for HPC (8.8%, i.e. 20% less) actually leads to a very significant increase in the limit state (maximum deviatoric stress), of near 2.5 times the LPC limit deviatoric stress value.

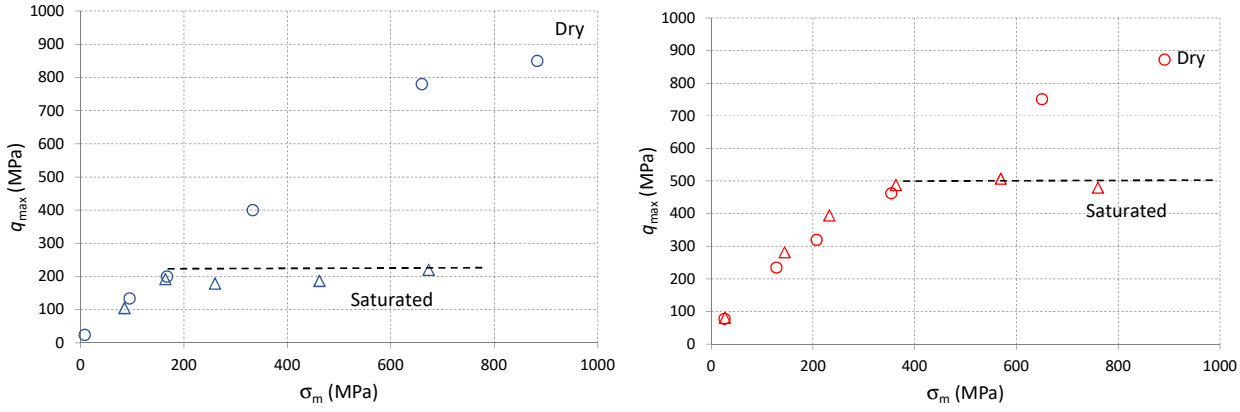

Fig. 9: Limit state curves of maximum deviatoric stress q_{max} vs. mean stress σ_m at two saturation states for LPC (highest porosity) (left) and HPC (lowest porosity) (right).

Fig. 10 plots the evolution in $q_{max,dry}/q_{max,sat}$ ratio vs. confining pressure p for all concretes where $q_{max,dry}$ is the maximum deviatoric stress for dry concretes, and $q_{max,sat}$ the maximum deviatoric stress for saturated concretes shown on Figs. 7

and 9. This evolution allows quantifying the gain in deviatoric stress when ~~incorporating the saturation state compared to~~ comparing the dry state (an *Sr* value of about 10%) to the saturated state. As shown in Fig. 6, note that the so-called "high performance concrete" (HPC with the lowest porosity) indicates a very different maximum saturated deviatoric stress value (between 2 and 2.5 times the limit values for OC and LPC).

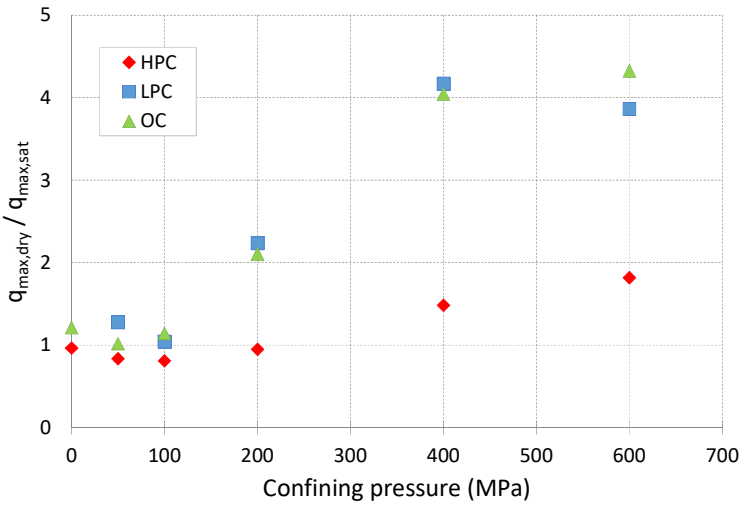

Fig. 10: Limit state curves of dry concrete relative to the maximum deviatoric stress of saturated concretes - $q_{max,dry}/q_{max,sat}$ vs. confining pressure p for all tested concretes (LPC, OC, HPC).

~~**Fig. 11:** Failure patterns for dry and saturated specimens after triaxial testing for LPC (a) and HPC (b)~~

~~The failure patterns after unloading of the triaxial test are displayed in Figure 11. It can be observed that for the HPC concrete, the same pattern appears for both saturated and dry concrete at a confining pressure below 100 MPa (behavior is being governed by the cement matrix). Above this confining pressure, the specimen tested already presents horizontal cracks (perpendicular to the loading) for the saturated concrete, whereas inclined macrocracks subsist for the dry specimen. It is clear therefore that water plays a role in the failure pattern whenever the cement paste cohesion decreases due to an increase in effective stress on the concrete. For LPC, horizontal cracks appear for both saturated and dry specimens at low pressure (50 MPa). Nevertheless, the number of horizontal cracks seems to be higher for dry concrete, and moreover the aggregate/cement paste debonding is limited by the presence of water.~~

6. Concrete failure criteria accounting for porosity and saturation ratio

This section will demonstrate what type of failure criterion can be identified from the experimental results presented in this paper. The effect of porosity will first be discussed using the results on concrete samples that have dried (i.e. saturation ratio *Sr* of about 10%). These limit states will then be compared to the one obtained on fully saturated samples (*Sr* = 100%). In the last part of this section, the results obtained for intermediate saturation ratios will be used

to propose a general empirical criterion that takes into account: unconfined concrete strength, concrete porosity, and its saturation ratio.

6.1. Discussion of failure surface criteria for high confined concretes at low saturation ratios

The failure surface area of concrete has been described in various ways for the purpose of numerical modeling. In the most common models, three kinds of meridian cross-sections of the failure surface, $q_{max}(\sigma_m)$, have been found: linear (Mohr-Coulomb, Druker-Prager [28], Willam-Warnke [29]), parabolic [30-34], or power law [35, 36]. A previous study [8] demonstrated that for mean stresses above 100 MPa, the limit state curve is nearly linear and the three types of failure criterion are very close. With lower mean stresses however, linear or parabolic criteria lead to overestimating the concrete strength. These criteria are incapable of fitting the unconfined compressive strength, whereas the power law is close to the measurements over all ranges. Let's assume that a power law criteria is indeed valid for all three concretes (LPC, OC and HPC):

$$q_{max} = a(b + \sigma_m)^{\alpha} \quad (2)$$

This criterion can also be written as follows:

$$q_{max} = q_1 \left(\frac{\sigma_0 + \sigma_m}{q_1}\right)^{\alpha} \quad (3)$$

where q_1 denotes a critical shear stress for which the criterion crosses the bisectrix and beyond which the maximum shear stress is less than the mean stress, with α being the slope of the criterion on the logarithmic scale, and σ_0 a reference mean stress that controls concrete shear strength at low mean stress levels.

Since their respective failure surfaces converge to the same surface as mean stress σ_m increases, parameters q_1 and α (or a and α) are assumed to be the same for all three concretes (i.e. not dependent on f_{ck}). These coefficients should primarily depend on the behavior of the fully compacted concrete, called granular stacking (aggregates + cement past without any strength or residual porosity), whereas parameter σ_0 (or b) should be a characteristic of the undamaged cement paste strength (material cohesion or f_{ck}). Figure 12 shows that such an assumption is in agreement with the experiments: the limit states of 5 types of concretes are very close to that of a power law criterion with a unique set of coefficients (q_1 = 980 MPa and α = 0.81). The 5 types of concretes considered herein (OC, HPC, LPC from the current study, and EC04, EC08 from a previous study) have very different unconfined compressive strengths and porosities, yet their granular stackings closely resemble one another.

To draw Fig. 12, the reference mean stress σ_0 has been deduced for each concrete mix design from ~~the~~ unconfined compressive tests. For such tests, the maximum deviatoric stress q_{max} is actually equal to the unconfined compressive ~~stress~~ strength f_{ck}, whereas the mean stress corresponds to one-third of this same value, hence:

$$\sigma_0 = q_1 \left(\frac{f_{ck}}{q_1}\right)^{1/\alpha} - \frac{f_{ck}}{3} \quad (4)$$

This relation, which yields a zero value for σ_0 if f_{ck} equals zero, is ~~in agreement with~~ deduced from Equation (3). It is in agreement with the case of a non-cohesive material (zero f_{ck} value) that should imply a shear strength q_{max} equal to zero under a mean stress σ_m also equal to zero. Lastly, combining Equations (3) and (4) produces a two-parameter law (q_1 and α) capable of predicting the failure criterion of concrete in the (q_{max}, σ_m) plane versus the unconfined compressive strength f_{ck}.

$$q_{max} = q_1 \left(\frac{\sigma_m - f_{ck}/3}{q_1} + \left(\frac{f_{ck}}{q_1}\right)^{1/\alpha}\right)^{\alpha} \quad (5)$$

This criterion can reproduce the failure of 5 very distinct concrete mix designs, from an f_{ck} of 21 MPa to 80 MPa, with a mean discrepancy between experiments and models of less than 5% (maximum discrepancy of 10%) and for a mean stress level ranging from 7 MPa to 1,000 MPa (see Fig. 12). It is also worth mentioning that parameters q_1 and α, which are constant in this paper, should probably change with the granular stacking (aggregate size or volume [9], aggregate type [37], etc.).

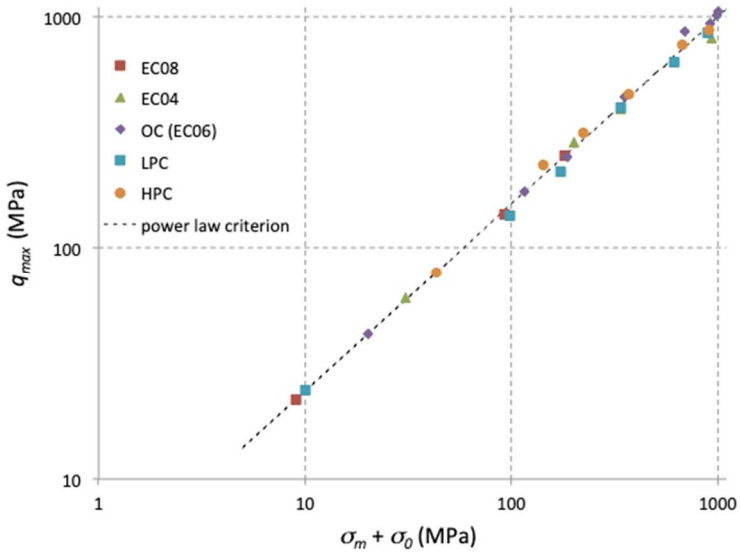

Fig. 12: Regression analysis between maximum experimental deviatoric stress q_{max} and mean stress ($\sigma_m + \sigma_0$) (EC04 and EC08, extracted from [8]), using the power law criterion given in Equation (4)

6.2. Effect of porosity on saturated concrete failure criteria

Figures 13 through 15 present the limit state curves of OC, HPC and LPC concretes, respectively, for both the dry (an *Sr* about 10%) and saturated concretes (*Sr* = 100%). These curves show that regardless of concrete porosity, at a low mean stress the maximum deviatoric stress q_{max} does not depend on the saturation ratio, while beyond a critical mean stress level $\sigma_{c_{sat}}$, q_{max} remains almost constant, and is defined as q_{sat}, for saturated concrete. As expected, the critical mean stress $\sigma_{c_{sat}}$ decreases with concrete porosity and especially with capillary porosity, as proven by the difference between the value of $\sigma_{c_{sat}}$ for HPC (397 MPa) and this same value for OC (143 MPa) or LPC (129 MPa). Knowing both the capillary (Φ_{cap}) and entrained air porosity (Φ_{air}) of the three concretes, the following three-parameter law enables reproducing the experiments quite well:

$$\sigma_{c_{sat}} = \sigma_{c_{p0}} - \lambda\phi_{air}^{1/3} - \kappa\phi_{cap}^{1/3} \quad (6)$$

where $\sigma_{c_{p0}}$ (approx. 1,280 MPa) is an ultimate consolidation stress; moreover, λ (approx. 210 MPa) and κ (approx. 2,350 MPa) are parameters that control the decrease in critical mean stress $\sigma_{c_{sat}}$ as the entrained air porosity or capillary porosity respectively increases. According to these results, the effect of capillarity porosity is roughly 10 times higher than that of the entrained air porosity. This result is consistent with the observations of porosity closure by Poinard *et al.* [38]. A comparison drawn between experiments and empirical criteria given by Equations (5) and (6) is depicted in Figures 13 through 15 for the three concretes using the unique set of parameters given in Table 2.

Table 2: Set of fitting parameters for the criterion given in Equations (5) and (6) and shown in Figures 13 to 15

Variable	Symbol	Value
Critical shear stress of dry concrete	q_1	980MPa
Slope of the criterion on a logarithmic scale	α	0.81
Ultimate consolidation stress	$\sigma_{c_{p0}}$	1280 MPa
Entrained air coefficient	λ	210 MPa
Capillary porosity coefficient	κ	2350 MPa

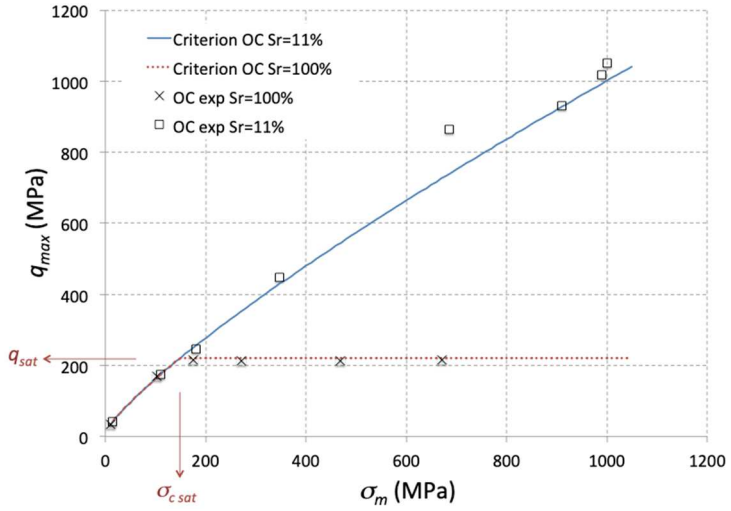

Fig. 13: Limit state curves of ordinary concrete (OC): maximum deviatoric stress q_{max} vs. mean stress σ_m; experimental results (dots); and analytical criterion (solid lines) for saturation ratios of Sr = 11% and Sr = 100%

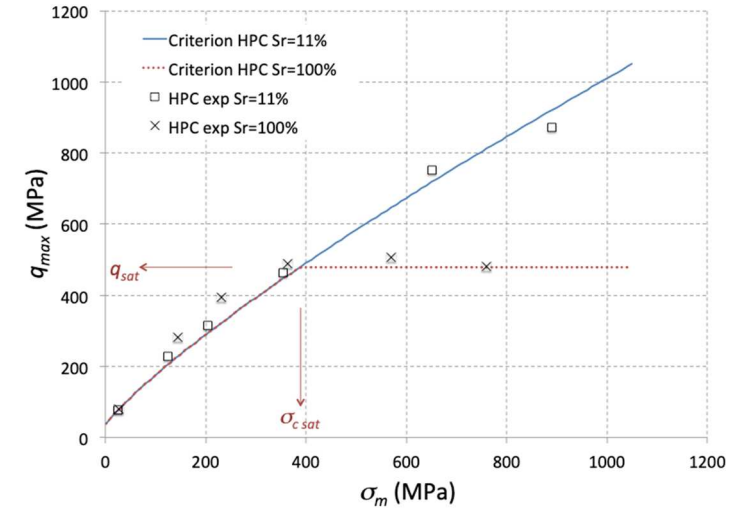

Fig. 14: Limit state curves of high performance concrete (HPC): maximum deviatoric stress q_{max} vs. mean stress σ_m; experimental results (dots), and analytical criterion (solid lines) for saturation ratios of Sr = 11% and Sr = 100%

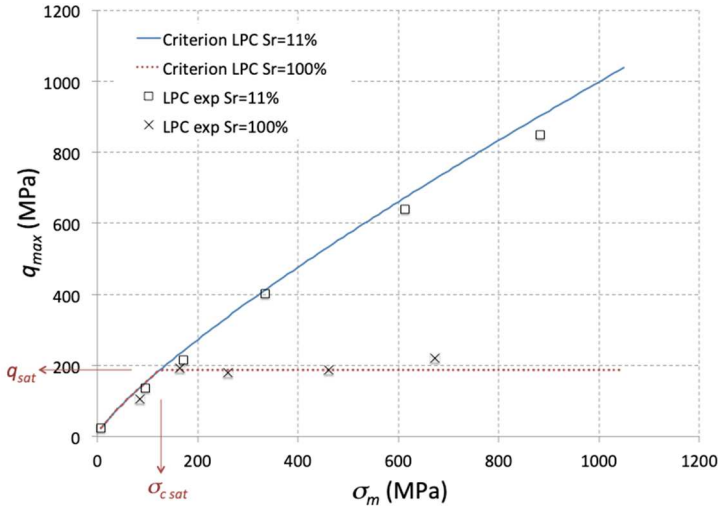

Fig. 15: Limit state curves of low performance concrete (LPC): maximum deviatoric stress q_{max} vs. mean stress σ_m; experimental results (dots) and analytical criterion (solid lines) for saturation ratios Sr = 11% and Sr = 100%

6.3. Case of ordinary concrete with different saturation ratios

Figure 16 shows that the observation recorded for saturated concretes in Section 6.2 is also satisfied for intermediate saturation ratios. In an initial approximation, at a low mean stress level, the maximum deviatoric stress q_{max} does not depend on the saturation ratio, whereas beyond a critical mean stress level, q_{max} remains just about constant, equal to q_{sr}, regardless of the mean stress level. Fig. 8 presents the evolution in this plateau value q_{sr} with respect to the saturation ratio S_r for ordinary concrete. This figure shows a monotonous decrease of q_{sr} versus S_r, with a small yet significant curvature. As an initial approximation, the following parabolic law provides a satisfactory estimation of the experimental values:

$$q_{sr}(S_r) = q_0 - \frac{S_r}{2}(3 - S_r)(q_0 - q_{sat}) \tag{7}$$

where q_{sat} and q_0 represent the levels of the criterion plateau when the concrete is saturated (S_r=100%) and fully dry (S_r=0%), respectively. Let's point out that Equation (7) does not add any new parameter. First, q_{sat} is already known from Equations (6) and (5):

$$q_{sat} = q_1 \left(\frac{\sigma_{cp0} - \lambda\, \phi_{air}^{1/3} - \kappa\, \phi_{cap}^{1/3} - f_{ck}/3}{q_1} + \left(\frac{f_{ck}}{q_1}\right)^{1/\alpha} \right)^{\alpha} \tag{8}$$

Second, let's assume that q_0 corresponds to an upper limit shear stress impossible to exceed and associated with complete closure of the concrete pores when the concrete is fully dry. Since a concrete without any air or capillary

porosity should behave independently of the saturation ratio, this upper limit q_0 can also be associated with the ultimate consolidation stress $\sigma_{c_{p0}}$ by using Equation (5) and neglecting f_{ck} in this equation ($\sigma_{c_{p0}} \gg f_{ck}$):

$$q_0 \approx q_1 \left(\frac{\sigma_{c_{p0}}}{q_1}\right)^{\alpha} \tag{9}$$

q_0 is then assumed to be the same for all concretes with the same granular stacking independently of their strength, as is the case for all the concrete mix designs introduced herein. The comparison between experiments and Equation (7) presented in Fig. 8 is obtained by using q_{sat} and q_0 from Equations (8) and (9), resulting in a good level of agreement.

Figure 16 presents a comparison between the proposed criterion and experiments for ordinary concrete at various saturation ratios. The good agreement observed in Fig. 16 reflects the pertinence of this failure criterion defined via Equations (5) to (9). This 5-parameter criterion (Table 2) lays out a general law that takes into account the concrete uniaxial strength, its porosity and its saturation ratio, i.e. the three most important properties for characterizing concrete shear strength with a mean stress level ranging from unconfined to 1 GPa.

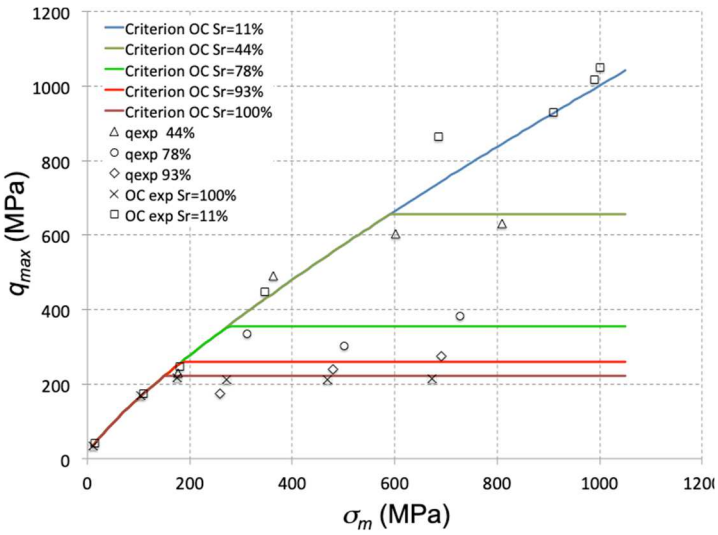

Fig. 16: Limit state curves of ordinary concrete (OC): maximum deviatoric stress q_{max} vs. mean stress σ_m; experimental results (dots); and analytical criterion (solid lines) for 5 saturation ratios ranging from Sr=11% to Sr=100%

7. Conclusion

This study has related the influence of porosity and free water to the behavior of concrete under high confinement. Triaxial tests have been conducted on three types of concrete, with either low, ordinary or high porosities, yet with the same aggregate skeleton, namely: an ordinary concrete (OC) characterized in previous studies, a high performance

concrete (HPC) with very low capillary porosity, and a low performance concrete (LPC) with a much higher entrained air porosity.

The results of confined compression tests, run up to a confinement of 600 MPa, at both low and high saturation ratios, made it possible to extend the conclusions drawn from previous studies on OC to the cases of HPC and LPC. Free water exerts a major influence on both the concrete strength capacity and the volumetric stiffness for all three types of concretes. A strong decrease in shear strength and an increase in the tangent bulk modulus are observed at high mean stress levels due to the presence of free water. These results also highlight that the free water influence on concrete behavior depends on the amount and type of porosity: the effect of modifying the entrained air porosity is much weaker than that of capillary porosity. More specifically, the decrease in capillary porosity leads to a higher critical mean stress, beyond which the shear strength of saturated specimens no longer increases. The effect of free water on the behavior of concretes with low capillary porosity is thus smaller than that previously observed for ordinary concretes. In contrast, an increase in entrained air porosity does not seem to exert any significant influence.

To better quantify the effect of concrete saturation ratio, triaxial tests performed on OC with intermediate homogeneous saturation ratios were also presented. Thanks to all these new results, an empirical triaxial failure criterion of concrete that takes into account uniaxial strength, porosity and saturation ratio was proposed. This new criterion serves to accurately reproduce the new results presented in the paper, as well as a large database obtained from previous studies.

8. Acknowledgments

The GIGA press was installed in the 3SR Laboratory within the framework of a cooperative agreement signed with the French Ministry of Defense. This research program could be performed thanks to financial support received from the French Alternative Energies and Atomic Energy Commission (CEA Gramat). The authors would also like to thank Dr. Benjamin Erzar, Jean-Luc Descone and Jean-Benoît Toni for their scientific and technical advices.

9. References

[1] L. Daudeville, Y. Malecot (2011) Concrete structures under impact. *European Journal of Environmental and Civil Engineering* 15(1): 101–140

[2] J. K. Gran, D. J. Frew (1997) In-target radial stress measurements from penetration experiments into concrete by ogive-nose steel projectiles, *International Journal of Impact Engineering*, 19(8): 715-726

[3] V. Baroghel-Bouny, M. Mainguy, T. Lassabatere, O. Coussy (1999) Characterization and identification of equilibrium and transfer moisture properties for ordinary and high-performance cementitious materials, *Cement and Concrete Research*, 29(8): 1225-1238

[4] H. Wang, L. Wanga, Y. Song, J. Wang (2016) Influence of free water on dynamic behavior of dam concrete under biaxial compression, *Construction and Building Materials*, 112: 222-231

[5] J. Zhou, X. Chen, L. Wu, X. Kan (2011) Influence of free water content on the compressive mechanical behaviour of cement mortar under high strain rate, *Sadhana* Vol. 36, Part 3, June 2011, pp. 357–369, Indian Academy of Sciences

[6] P. Forquin, K. Safa, G. Gary (2010) Influence of free water on the quasistatic and dynamic strength of concrete in confined compression tests, *Cement and Concrete Research,* 40(2): 321–333

[7] E. Piotrowska, P. Forquin, Y. Malecot (2016) Experimental study of static and dynamic behavior of concrete under high confinement: Effect of coarse aggregate strength, *Mechanics of Materials*, 92: 164-174

[8] X. H. Vu, Y. Malecot, L. Daudeville, E. Buzaud (2009) Effect of the water/cement ratio on concrete behavior under extreme loading, *International Journal for Numerical and Analytical Methods in Geomechanics*, 33(17):1867-1888

[9] X. V. Vu, L. Daudeville, Y. Malecot (2011) Effect of coarse aggregate size and cement paste volume on concrete behaviour under high triaxial compression loading. *Construction and Building Materials*, 25(10): 3941–3949

[10] L. Zingg, M. Briffaut, J. Baroth, Y. Malecot (2016) Influence of cement matrix porosity on the triaxial behaviour of concrete, *Cement and Concrete Research*, 80: 52-59

[11] X. V. Vu, Y. Malecot, L. Daudeville, E. Buzaud (2009) Experimental analysis of concrete behaviour under high confinement: Effect of the saturation ratio, *International Journal of Solids and Structures*, 46(5): 1105-1120

[12] T. Gabet, Y. Malecot, L. Daudeville (2008) Triaxial behaviour of concrete under high stresses: influence of the loading path on compaction and limit states, *Cement and Concrete Research,* 38(3): 403-412

[13] X. V. Vu, Y. Malecot, L. Daudeville (2009) Strain measurements on porous concrete samples for triaxial compression and extension test under very high confinement, *Journal of Strain Analysis for Engineering Design*, 44(8): 633-657

[14] Y. Malecot, L. Daudeville, F. Dupray, C. Poinard, E. Buzaud (2010) Strength and damage of concrete under high triaxial loading, *European Journal of Environmental and Civil Engineering*, 14(6): 777–803

[15] X.-D.Vu, M. Briffaut, Y. Malecot, L. Daudeville, B. Ciree (2015) Influence of the Saturation Ratio on Concrete Behaviour under Triaxial Compressive Loading, *Science and Technology of Nuclear Installations,* Article ID 976387, http://dx.doi.org/10.1155/2015/976387

[16] CEN: EN-1992-1-1. Eurocode 2. Design of concrete structures – Part 1-1. General rules and rules for buildings, 2004

[17] *fib:* Model Code 2010, final draft. 2012. Bulletin n°65 & 66, 2012

[18] M. Jirasek, Z. P. Bažant (2002) Inelastic Analysis of Structures, John Wiley & Sons

[19] P.-C. Aïtcin (1983) Condensed Silica Fumes, University of Sherbrooke, Québec, Canada, ISBN 2-7622-0016-4, 52p

[20] F. De Larrard (1999) Concrete Mixture-Proportioning - A Scientific Approach, *Modern Concrete Technology Series*, n°9, E & FN SPON, Londres

[21] P. K. Metha (1986) Concrete structures, properties, and materials. Prentice-Hall, 450 p

[22] S. Diamond (2000) Mercury porosimetry - an inappropriate method for the measurement of pore size distributions in cement-based materials, *Cement and Concrete Research*, 30(10): 1517-1525

[23] I. Yurtdas , N. Burlion, F. Skoczylas (2004) Triaxial mechanical behaviour of mortar: Effects of drying, *Cement and Concrete Research*, 34(7): 1131-1143

[24] N. Burlion (2010), Caractérisation du comportement hydrique du béton R30A7 et prévision de son comportement mécanique, rapport de contrat CEA Gramat - DGA n°200725100000510000

[25] L. Zingg, Y. Malecot, M. Briffaut, J. Baroth, S. Pla (2016) A Radial Strain Sensor for the Characterization of Concrete Under Triaxial Loading , *Experimental Mechanics*, 56(5): 703-711

[26] B. Nedjar (2014) On finite strain poroplasticity with reversible and irreversible porosity laws. Formulation and computational aspects, *Mechanics of Materials*, 68: 237-252

[27] O. Coussy (1995) Mechanics of Porous Continua, John Wiley & Sons, New York, NY, USA.

[28] D.C. Drucker, W. Prager (1952) Soil mechanics and plastic analysis on limit design, *Quaterly of Applied Mathematics*, 10(2): 157-165

[29] K. Willam, E. P. Warnke (1974) Constitutive model for the triaxial behaviour of concrete, *International Association of Bridge and Structural Engineers Seminar on Concrete Structures Subjected to Triaxial Stresses*, Paper III-1. Bergamo

[30] F. Schleicher (1926) Der Spannungszustand an der Fliessgrenze (Plastizitätsbedingung), *Zeitschrift für angewandte Mathematik und Mechanik*, 6: 199–216. 45 [in German]

[31] A. Nadai (1950) Theory of flow and fracture of solids. Vol. 1. McGraw-Hill, New York

[32] R. Krieg (1972) A simple constitutive description for soils and crushable foams. Report SC-DR-72-0883, Sandia National Laboratories, Albuquerque, 46, 94-168

[33] D. V. Swenson, L. M. Taylor (1983) A finite element model for the analysis of tailored pulse simulation of boreholes, *International Journal for Numerical and Analytical Methods in Geomechanics*, 7(4): 469–484

[34] C. Pontiroli, A. Rouquand, J. Mazars (2010) Predicting concrete behaviour from quasi-static loading to hypervelocity impact: an overview of the PRM model, *European Journal of Environmental and Civil Engineering*, 14(6–7): 703-727

[35] I. W. Johnston (1985) Strength of Intact Geomechanical Materials, *Journal of Geotechnical Engineering*, ASCE, 111(6): 730-748

[36] H. D. Kang, K. Willam (1999) Localization characteristics of triaxial concrete model, *Journal of Engineering Mechanics-ASCE*, 125(8): 941–950

[37] E. Piotrowska, Y. Malecot, Y. Ke (2014) Experimental investigation of the effect of coarse aggregate shape and composition on concrete triaxial behaviour, *Mechanics of Materials*, 79: 45-57

[38] C. Poinard, E. Piotrowska,, Y. Malecot, L. Daudeville, E. N. Landis (2012) Compression triaxial behavior of concrete: the role of the mesostructure by analysis of X-ray tomographic images, *European Journal of Environmental and Civil Engineering* 16(1): 115-136

[39] Cui, J., Hao, H., Shi, Y. (2018) Study of concrete damage mechanism under hydrostatic pressure by numerical simulations. *Constr. Build. Mater.* 160, 440–449. https: //doi.org/10.1016/j.conbuildmat.2017.11.083.

[40] Cui, J., Hao, H., Shi, Y., Li, X., Du, K. (2017) Experimental study of concrete damage under high hydrostatic pressure. *Cem. Concr. Res.* 100, 140–152. https://doi.org/ 10.1016/j.cemconres.2017.06.005.

[41] Karinski, Y.S., Yankelevsky, D.Z., Zhutovsky, S., Feldgun, V.R. (2017b) Uniaxial confined compression tests of cementitious materials. *Constr. Build. Mater.* 153, 247–260. https://doi.org/10.1016/j.conbuildmat.2017.07.010.

[42] Yankelevsky, D.Z., Karinski, Y.S., Zhutovsky, S. , Feldgun, V.R. (2018) High-pressure uniaxial confined compression tests of mortars. *Constr. Build. Mater.* 165, 523–532.

[43] Zhutovsky, S, Karinski, Y.S., Yankelevsky, D.Z., Feldgun V.R., Multiscale model for the prediction of equation of state for cement paste and mortar. *International Journal of Solids and Structures* 152–153 (2018) 324–335

[44] Sakai, Y, Nakatani, M, Takeuchi, A, Omorai, Y, Kishi, T (2016) Mechanical Behavior of Cement Paste and Alterations of Hydrates under High-Pressure Triaxial Testing, *Journal of advance Concrete Technology* 14(1):1-12